J. Fluid Mech. (1995), *vol.* 282, *pp.* 21–44

Two-dimensional flows with zero net momentum: evolution of vortex quadrupoles and oscillating-grid turbulence

By S. I. VOROPAYEV[1], Y. D. AFANASYEV[1] AND G. J. F. VAN HEIJST[2]

[1] Institute of Oceanology, Russian Academy of Sciences, Krasikova 23, Moscow 117851, Russia

[2] J. M. Burgers Centre for Fluid Mechanics, Department of Technical Physics, Eindhoven University of Technology, P.O. Box 513, 5600 MB Eindhoven, The Netherlands

(Received 15 September 1992 and in revised form 7 July 1994)

The planar flow arising in an initially quiescent viscous fluid under the action of a localized dipolar-type forcing has been studied analytically and experimentally. The force dipole, with non-dimensional forcing amplitude Re, brings net zero momentum into the fluid and gives rise to the formation of a quadrupolar vortex: a system of two dipolar vortices moving apart. Experimentally, the action of a force dipole was modelled by a vertical cylinder oscillating horizontally in the shallow upper layer of a two-layer fluid. Two cases were studied: single quadrupoles and an array of quadrupoles. It is found that single quadrupoles develop in a self-similar manner: the length L and the translation velocity $\bar{U}$ of the quadrupolar vortex change with time as $L \sim t^{1/2}$ and $\bar{U} \sim t^{-1/2}$. These quantities are characterized by non-dimensional functions $\alpha(Re)$ and $\beta(Re)$, respectively, which have been determined theoretically for small Re-values and experimentally for Re-values in the range 160–2200.

To produce an array of quadrupoles an array of oscillating vertical rods was used. Two stages in the flow evolution were studied experimentally: the initial stage, when the interactions between the quadrupoles are weak, and the intermediate stage when the interactions play an essential role and the flow is (two-dimensionally) turbulent. It is found that at both stages the width H of the region with intense vortical motions increases with time as $H \sim t^{1/2}$. A theoretical explanation of the experimental results is given.

1. Introduction

The dynamics of coherent vortex structures as commonly occur in geophysical flow situations have received considerable attention during the last few years. Theoretical, numerical and experimental studies have revealed the existence of a number of different vortex types: the monopolar vortex, characterized by a non-zero angular momentum; the dipolar vortex, with non-zero linear momentum; and the tripolar vortex, also characterized by a non-zero angular momentum. In many studies different analytical approximations are used to describe the dynamics of these compact vortices, without considering the physical formation mechanism causing these vortex structures to arise in an otherwise quiescent viscous fluid. The latter problem is closely related to the general problem of the generation of unsteady vortex multipoles by localized external forcing in an unbounded fluid (Cantwell 1986). Only for the simplest case of a symmetric vortex monopole has an exact unsteady nonlinear solution been found

(Afanasyev & Voropayev 1991). Such solutions for the higher-order vortex multipoles are as yet not known, as far as we are aware.

In view of the obvious difficulties in the analytical approach, laboratory experiments become very helpful in elucidating the physical mechanism of the formation of multipolar vortices and their subsequent evolution. The laboratory observations by Voropayev & Filippov (1985), Afanasyev, Voropayev & Filippov (1988), van Heijst & Flór (1989), Fernando, van Heijst & Fonseka (1992) and Flór & van Heijst (1994) have revealed that the dipole vortices induced by a localized force, acting either impulsively or continuously, develop in a self-similar manner. This allows a significant simplification of the interpretation of experimental data, and also enables one to construct semi-empirical models for this dipolar flow evolution (Voropayev, Afanasyev & Filippov 1991).

In addition to the fundamental vortex types mentioned above, there is another basic vorticity structure: the quadrupolar vortex, consisting of two dipoles moving apart. This more complicated structure was considered by Voropayev & Afanasyev (1992), aiming at the interpretation of the experimental results of dipole–dipole interactions as well as the interaction of a dipole with a solid boundary. In its archetypal form, a vortex quadrupole is generated by the action of a localized force dipole in a viscous fluid and the total momentum of the flow induced by this source is zero. Although a self-similar solution for the initial stage of the quadrupole evolution shows qualitative agreement with the laboratory observations of Voropayev & Afanasyev (1992), a systematic quantitative study of these flow structures has not yet been performed, and analytical or semi-empirical models are barely developed. It is the main aim of this paper to provide these: below, the characteristics of vortex quadrupoles are analysed theoretically for small Re-values and investigated experimentally for larger Re-values, where Re is the non-dimensional forcing amplitude. In the experiments the action of a localized force dipole on the fluid was modelled by a vertical cylinder oscillating horizontally in the shallow upper layer of a two-layer fluid. Averaged over the oscillation period, the cylinder exerts equal but oppositely directed forces on the fluid, thus effectively reproducing the action of a localized force dipole.

As a continuation of the study of the single quadrupolar vortex, an attempt was also made to reproduce an array of quadrupoles and to study the propagation dynamics of the two-dimensional turbulence that arises. For this purpose we used a linear grid of vertical rods oscillating horizontally in the shallow upper layer of the two-layer fluid in the direction normal to the plane of the grid. This experiment can be considered as a two-dimensional analogue of well-known experiments on three-dimensional turbulence induced by a planar horizontal grid oscillating vertically in a deep fluid tank.

The remainder of this paper is organized as follows. A preliminary analysis and some estimates of characteristic features of the flow are presented in §2. The experimental arrangement is described in §3. The experimental data on single quadrupoles are presented in §4.1, while experimental results obtained for the array of quadrupoles and the propagation of the two-dimensional turbulent region are discussed in §4.2. Finally, a comparison with experiments on three-dimensional oscillating-grid turbulence as well as the main conclusions of the present study are given in §5.

2. Preliminary analysis

Consider the planar unsteady flow of a viscous incompressible fluid (with density ρ and kinematic viscosity ν) induced by two identical point sources of momentum,

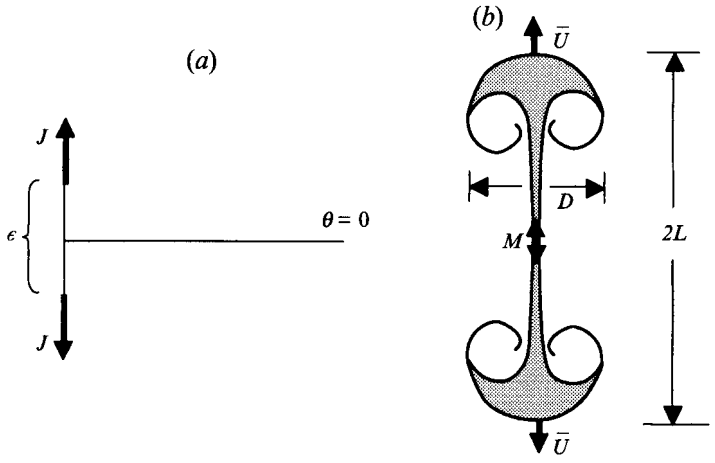

FIGURE 1. Schematic drawing of the momentum sources (*a*) and the quadrupolar vortex (*b*) arising under the action of two equal forces acting in opposite directions. The typical length L, width D and propagation velocity $\bar{U}(= \mathrm{d}L/\mathrm{d}t)$ of the evolving flow structure are defined as indicated in the figure.

exerting on the fluid equal forces $J\rho$ in opposite directions. As indicated schematically in figure 1, the momentum sources are located a distance ϵ apart. In a polar coordinate system (r, θ), their positions are $(\frac{1}{2}\epsilon, \frac{1}{2}\pi)$ and $(\frac{1}{2}\epsilon, -\frac{1}{2}\pi)$ and the forces are exerted in opposite directions $\theta = \frac{1}{2}\pi$ and $\theta = -\frac{1}{2}\pi$, respectively. By decreasing the distance ϵ and simultaneously increasing the force amplitude J in such a way that their product $\epsilon J = M$ remains constant, one obtains a point force dipole of intensity $M\rho$ at the origin $r = 0$. It is assumed that the fluid is initially at rest and extends to infinity. The source of intensity $M = \text{const.}$ starts at $t = 0$ and the dimensions of M are L^4T^{-2}. The resulting planar motion can be expressed in terms of the vorticity ω (in fact the vorticity component perpendicular to the flow plane) and the stream function ψ, which is defined through $\boldsymbol{v} = -\boldsymbol{k} \times \nabla\psi$, with $\boldsymbol{k}$ the unit vector perpendicular to the flow plane. Solving the linear equation for the vorticity

$$\partial\omega/\partial t = \nu\nabla^2\omega$$

and then the Poisson equation for the stream function

$$\nabla^2\psi = -\omega,$$

one obtains the solution of this problem in the Stokes approximation (Voropayev & Afanasyev 1992):

$$u = \frac{1}{r}\frac{\partial\psi}{\partial\theta} = -Re\frac{\nu}{r}\xi^{-2}\{1 - \exp(-\xi^2)\}\cos 2\theta, \tag{1a}$$

$$v = -\frac{\partial\psi}{\partial r} = -Re\frac{\nu}{r}\{\xi^{-2} - (1 + \xi^{-2})\exp(-\xi^2)\}\sin 2\theta. \tag{1b}$$

where u and v are the radial and azimuthal velocity components, respectively, ξ is the non-dimensional similarity variable

$$\xi = r/2(\nu t)^{1/2} \tag{2}$$

and Re is the non-dimensional forcing defined as

$$Re = M/4\pi\nu^2. \tag{3}$$

Solution (1) describes the evolution of a vortex flow arising in initially quiescent fluid. This flow represents two symmetric dipolar vortices moving apart in the directions $\theta = \pm\frac{1}{2}\pi$ (see figure 1) and we set out to calculate the maximum length L and width D of the flow pattern visible in the fluid of a passive tracer that was initially released in the vicinity of the source. This calculation can be performed as follows. For $r < r_0$ and $t \gg r_0^2/\nu$, with r_0 an arbitrary constant radius, the solution can be expanded in a power series in ξ (for small ξ-values). Taking the limit $\xi \to 0$ in (1), one obtains

$$\lim_{\xi \to 0} \{u, v\} = \left\{ -\frac{Re\,\nu}{r} \cos 2\theta, 0 \right\}.$$

This result implies that the radial velocity decreases with distance as r^{-1}, while the azimuthal velocity vanishes at the ultimate steady stage of the flow evolution. In view of this, it is now assumed that the characteristic velocity U_0 in the flow can thus be estimated as

$$U_0 = Re\,\nu/r. \tag{4}$$

This is in accordance with general principles of similarity (see e.g. Sedov 1959): the problem has no external lengthscale and the only scale is the distance r from the origin. In a self-similar flow

$$D = \alpha L, \tag{5}$$

where α is a non-dimensional function that does not depend on the distance r, but which may depend only on the Reynolds number, which at $r = L$ is equal to the non-dimensional forcing:

$$Re = U_0 L/\nu = M/4\pi\nu^2. \tag{6}$$

By scaling the flow velocity field by U_0, the velocity $\bar{U}$ of the vortex front moving into the ambient quiescent fluid (see figure 1) can be estimated in a similar fashion:

$$\bar{U} = \mathrm{d}L/\mathrm{d}t = \beta U_0, \tag{7}$$

where β is also a non-dimensional function of Re. Combination of (4) and (7) for $r = L$ yields

$$L = (2\beta\, Re\, \nu t)^{1/2}. \tag{8}$$

By using (1) it is possible to calculate $\beta(Re)$ and $\alpha(Re)$.

With the help of the similarity variable (2), the equations of motion for marked fluid particles

$$\frac{\mathrm{d}r}{\mathrm{d}t} = u, \quad \frac{\mathrm{d}\theta}{\mathrm{d}t} = \frac{v}{r},$$

with u and v given by (1), can be presented in a non-dimensional form:

$$\mathrm{d}\xi/\mathrm{d}\tau = -\tfrac{1}{4} Re\, \xi^{-3} \{1 - \exp(-\xi^2)\} \cos 2\theta - \tfrac{1}{2}\xi, \tag{9a}$$

$$\mathrm{d}\theta/\mathrm{d}\tau = -\tfrac{1}{4} Re\, \xi^{-2} \{\xi^{-2} - (1 + \xi^{-2}) \exp(-\xi^2)\} \sin 2\theta, \tag{9b}$$

where $\tau = \ln t$. The points where $\mathrm{d}\xi/\mathrm{d}\tau = \mathrm{d}\theta/\mathrm{d}\tau = 0$ determine the positions of the critical stagnation points where the non-dimensional velocities (9) are equal to zero, thus giving the positions of the dyed fronts of the flow. Two symmetrical stagnation points ($\xi = \xi_0, \theta = \pm\frac{1}{2}\pi$) at the leading fronts of the flow are clearly seen from the system (9), with the value of $\xi = \xi_0$ being determined by the equation

$$\tfrac{1}{2} Re\, \xi_0^{-3} \{1 - \exp(-\xi_0^2)\} = \xi_0. \tag{10}$$

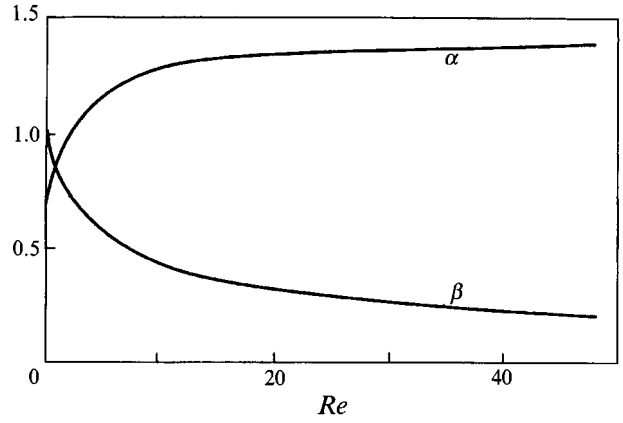

FIGURE 2. Functions $\alpha(Re)$ and $\beta(Re)$ calculated from solution (1) for small Re-values.

From (1*a*) and (10) we obtain for the propagation velocity $\bar{U}$ of the leading fronts

$$\bar{U} = U(\xi_0, \theta = \pm\tfrac{1}{2}\pi, t) = (\nu/t)^{1/2}\,\xi_0, \tag{11}$$

or in equivalent form

$$\bar{U} = 2(\nu/r)\,\xi_0^2.$$

This gives the value for the propagation velocity of the front formed by dyed fluid particles which initially were at the vicinity of the source of motion. Scaling $\bar{U}$ by U_0 given by (4) yields

$$\beta = \bar{U}/U_0 = (2/Re)\,\xi_0^2. \tag{12}$$

By solving (10) one finds $\xi_0(Re)$ and obtains the function $\beta(Re)$, which is shown graphically in figure 2 for small Re-values.

The maximum width D of the dyed pattern is determined by calculating the positions of the points at which the velocity component perpendicular to the axis of the flow changes its sign. This gives the condition

$$\frac{\mathrm{d}}{\mathrm{d}\tau}(\xi\cos\theta) = \cos\theta\frac{\mathrm{d}\xi}{\mathrm{d}t} - \xi\sin\theta\frac{\mathrm{d}\theta}{\mathrm{d}t} = 0,$$

which determines the curve

$$\theta = \arcsin\left[\frac{2\xi^4\,Re^{-1} + 1 - \mathrm{e}^{-\xi^2}}{2\{2(1-\mathrm{e}^{-\xi^2}) - \xi^2\,\mathrm{e}^{-\xi^2}\}}\right]^{1/2}. \tag{13}$$

The distance between two symmetrical points (ξ^0, θ^0), $(\xi^0, \pi - \theta^0)$ on this curve, which have a maximum distance from the axis of the flow, gives the value of the width D of the dyed pattern (see figure 3)

$$D = 2(\nu t)^{1/2}(2\xi^0\cos\theta^0).$$

Combination of this result with (5), (8) and (12) yields the function $\alpha(Re)$, i.e.

$$\alpha(Re) = D/L = 2(\xi^0/\xi_0)\cos\theta^0, \tag{14}$$

and its behaviour as calculated from (10) and (13), is shown graphically in figure 2.

The estimates obtained are valid for small Re-values when the flow, determined by

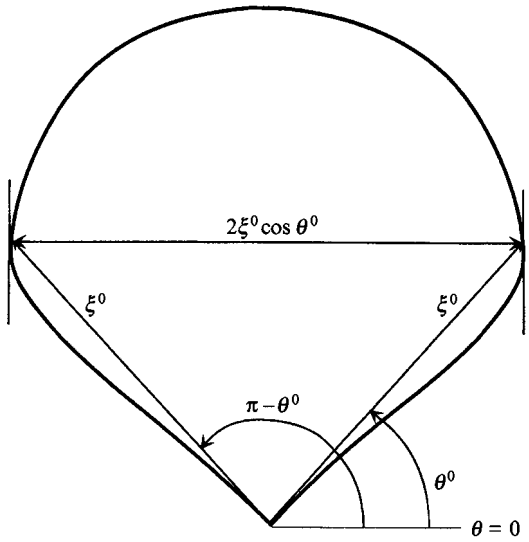

FIGURE 3. Explanatory sketch for the upper part of curve (13) in self-similar polar coordinates (ξ, θ) for $Re = 20$. Near the points (ξ^0, θ^0) and $(\xi^0, \pi-\theta^0)$ the fluid particles cannot cross this curve and the distance $D/2\nu^{1/2}t = 2\xi^0\cos\theta^0$ between these points determines the maximum width D of the flow pattern.

(1), is self-similar. The validity of (5) and (8), i.e. self-similarity, for large Re-values must be verified experimentally. On general grounds one may only expect that when nonlinear effects become dominant $\alpha(Re)$ decreases for increasing Re-values and $\alpha(Re)\to 0$ as $Re\to\infty$ (see e.g. Batchelor 1967), but $\beta(Re)\to\frac{1}{2}$ as $Re\to\infty$ (see Stern & Voropayev 1984). Below, the validity of (5) and (8) is verified experimentally and the functions α and β are determined for large Re-values.

3. Description of the experiment

The majority of the laboratory experiments were performed in a glass rectangular container (35 cm × 30 cm) with a working depth of 3 cm. To control the possible influence of the container size on the flow characteristics, some additional experiments were performed in a larger container (55 × 65 cm). In order to reproduce nearly two-dimensional flow, the container was filled with two layers of immiscible fluids of different density. The lower layer was relatively deep (approximately 2 cm) and contained heavy CCl_4, and this fluid was topped by a shallow (0.4 cm) layer of distilled water. Because of the lower viscosity of CCl_4, the flow induced in the upper layer was thus 'shielded' from the bottom, i.e. the bottom friction was effectively reduced by the presence of the lower layer. To reduce the effect of surface tension, some drops of shampoo were added to the surface of the upper layer and to the interface between the upper and lower layers. After this the flow induced in the upper layer was almost vertically uniform over its depth, and therefore to a very good approximation two-dimensional. Strictly speaking, the motion in the upper layer is only planar (horizontal), but three-dimensional, because the vertical vortex lines in the upper layer are closed at the upper and lower surfaces of the upper layer. But neglecting this, it can to a good approximation be considered as two-dimensional or at least as quasi-two-dimensional.

The motions were visualized by adding the pH-indicator thymol blue to the upper fluid, which – after the addition of some acid – was coloured yellow. Addition of a few

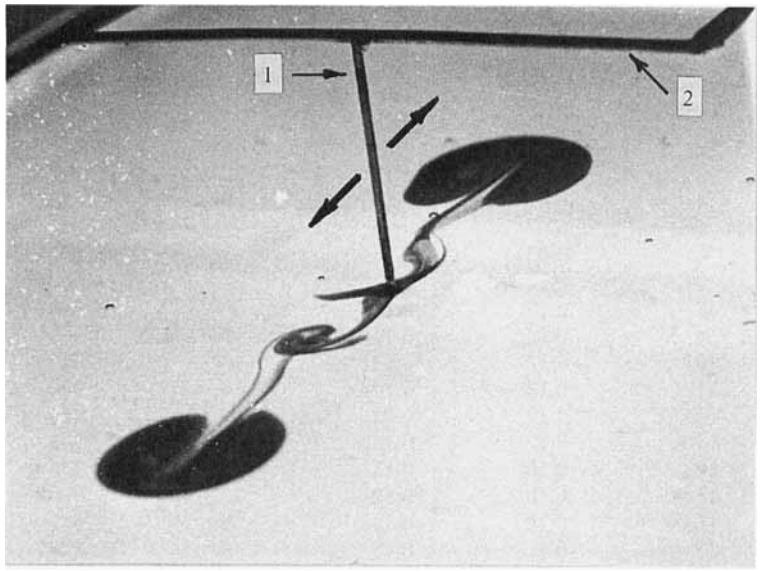

FIGURE 4. Oblique view of the generation mechanism and the resulting quadrupolar flow in the shallow layer of distilled water floating on top of a deeper layer of CCl_4. The vertical rod 1, connected to a loudspeaker by a horizontal frame 2, performs harmonic oscillations in the horizontal directions indicated by the arrows. The flow is visualized by the thymol-blue technique (see text).

drops of slightly basic water turned the colour locally to dark blue, thus providing a good contrast. In each experiment only a few drops of basic fluid were introduced in the flow area of interest. After an experiment it took only a few minutes for the diffusive chemical reaction with the acidic ambient fluid to restore the original yellow colour of the upper layer, and the next experiment could be performed without changing the working fluid. The experimental data were mainly obtained through photographs of the visualized coloured flow patterns (see figures 4 and 5). Good contrast was obtained by illuminating the coloured fluid through the glass tank bottom by fluorescent lamps. In addition, streak photographs were taken, for which purpose the upper layer was seeded with small neutrally buoyant tracer particles. In this case the upper layer was illuminated by a horizontal light sheet produced from one side.

The quadrupolar flow in the upper layer was induced by so-called 'acoustic streaming'. The arrangement of this generation technique (see figure 4) consists of a rigid horizontal frame connected to a loudspeaker (one loudspeaker was used for the smaller container and two for the larger container), whose motion could be controlled by a function generator. The cylinder (in fact a thin rod of circular cross-section) is fixed to the supporting frame and is placed vertically in the upper fluid layer in the centre of the container such that its end almost touches the interface between the layers. In this way it was possible to let the cylinder perform horizontal oscillations in a sinusoidal fashion with adjustable frequency f and amplitude ϵ. In order to vary the effective size of the source of motion, experiments were performed with cylinders of different diameters d in the range 0.03–0.16 cm, whereas the amplitude ϵ of the oscillation was varied from 0.1–0.18 cm. The frequency f was taken either 9 or 18 Hz. The values of the experimental parameters are listed in table 1. Prior to each experiment a small area in the upper layer in the vicinity of the cylinder was dyed a contrasting dark blue colour by adding a few drops of basic fluid. In this way the resulting flow patterns could be visualized nicely, as can be seen in figures 5 and 6.

Experiment number	d(cm)	ϵ(cm)	f(Hz)	$Re = M/4\pi\nu^2$
1	0.03	0.186	9	156
2	0.07	0.095	18	270
3	0.07	0.12	18	430
4	0.07	0.143	9	215
5	0.07	0.15	9	240
6	0.07	0.184	9	356
7	0.12	0.095	18	460
8	0.12	0.103	9	190
9	0.12	0.12	9	260
10	0.12	0.12	18	735
11	0.12	0.143	18	1040
12	0.12	0.15	9	406
13	0.12	0.16	18	1306
14	0.16	0.12	9	346
15	0.16	0.12	18	980
16	0.16	0.138	9	460
17	0.16	0.15	9	540
18	0.16	0.175	9	736
19	0.16	0.184	9	814
20	0.16	0.18	18	2204
21	0.08	0.18	17	1010
22	0.08	0.14	18	667
23	0.24	0.1	17	935

TABLE 1. Experimental parameters for single quadrupoles. The uncertainty in measuring ϵ is about 1%, so the third number after the decimal point is not reliable. Experiments 21, 22 and 23 were performed in the larger container.

Qualitatively, the formation mechanism of these structures is rather simple (see e.g. Batchelor 1967). A small oscillating body in a viscous fluid generates layers of alternatingly positive and negative vorticity. Because convection carries some vorticity away from the boundary, not all the vorticity in these layers diffuses in such a way that oppositely signed vorticities cancel. This leads to the formation of a quadrupolar vorticity distribution near the body and, as a result, a vortex quadrupole arises in the initially still fluid. When a solid body oscillates back and forth about some mean position in a viscous fluid, it exerts a force on the latter in alternating directions. It can be shown (see e.g. Batchelor 1967) that the resulting force varies periodically with the frequency of oscillation of the body and consists of two parts: an inertial one and a dissipative one. The phase shift between the inertial force and the velocity of the body is $\frac{1}{2}\pi$, and therefore the inertial force does not increase the kinetic energy of the fluid. In contrast, the dissipative force that appears owing to the no-slip conditions at the body surface and the subsequent creation of a boundary layer on the body varies with the same phase as the velocity of the body. Only in some simple cases is it possible to estimate accurately the amplitude of the dissipative force. For example, for a cylinder of diameter d oscillating with a small amplitude ϵ in a direction perpendicular to its axis the mean amplitude of this force (per unit length of the cylinder) is given by (Batchelor 1967, p. 357)

$$\rho J = 4\pi^{5/2}\rho\, d\nu^{1/2}\,\epsilon f^{3/2}, \tag{15}$$

where f is the oscillation frequency in Hz (note that without this formula it is hardly possible to estimate correctly the value of J, which is a function of four independent

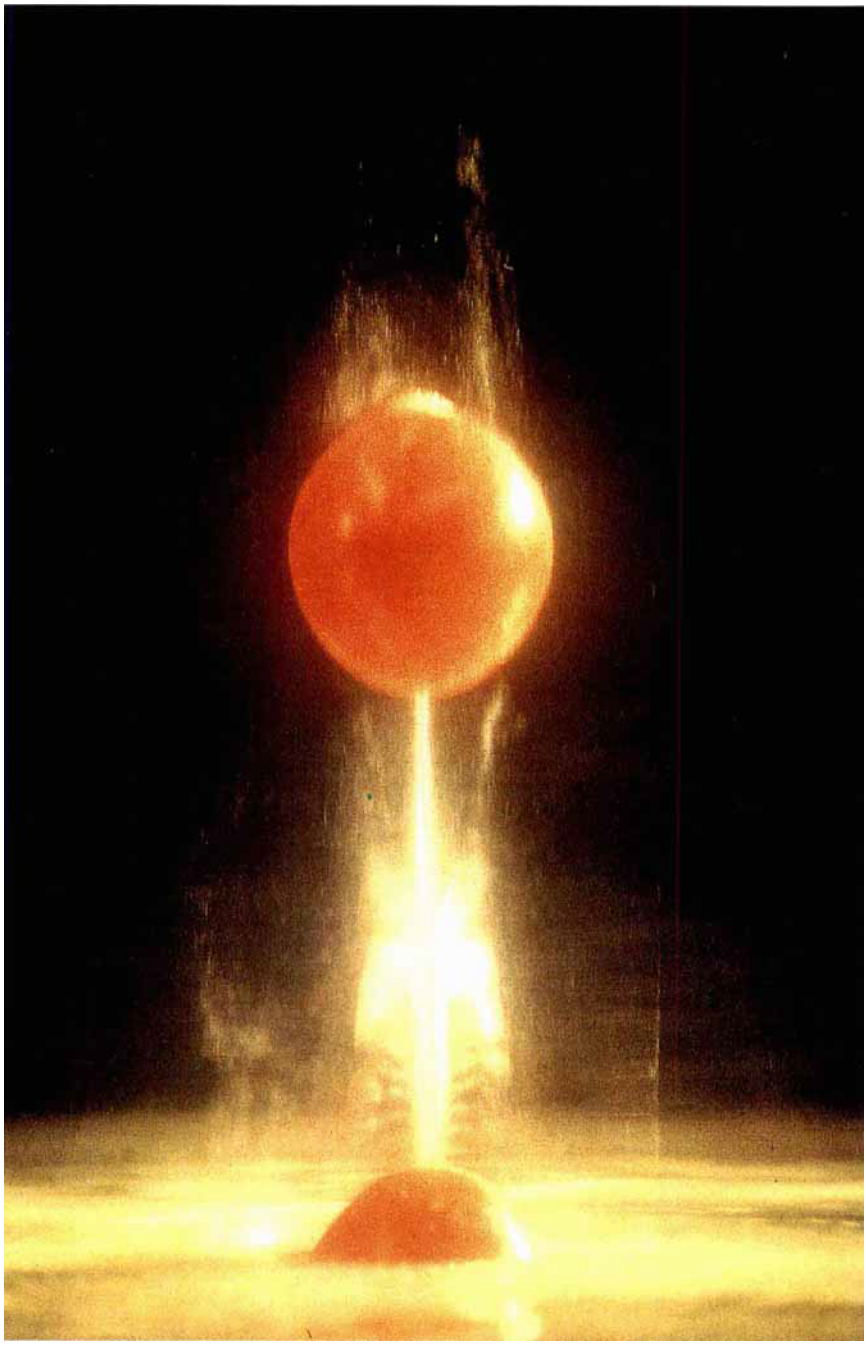

FIGURE 5. Colour picture of the vortex quadrupole (top view) induced by a continuously oscillating cylinder. In contrast to the pictures shown in figure 6, the ambient fluid is in the basic form (light blue). Prior to the experiment a small area in the vicinity of the cylinder was dyed by adding a few drops of acidic fluid.

Experiment number	Symbol	d_0 (cm)	ϵ (cm)	f(Hz)	$Re = M/4\pi\nu^2$	$t_*(s)$	$\Delta t(s)$
1	□	0.5	0.128	18	490	0.35	0
2	+	0.5	0.133	18	530	0.33	0
3	*	0.5	0.190	15	820	0.25	0
4	●	1	0.146	9	225	2.2	1
5	○	1	0.133	18	530	1.3	1
6	△	1	0.158	18	740	1.1	0.5
7	■	2	0.094	18	260	8.1	1
8	▲	2	0.133	18	530	5.3	1

TABLE 2. Experimental parameters for the array of quadrupoles. The uncertainty in measuring ϵ is about 1%, so the third number after the decimal point is not reliable.

parameters). The direction of this force changes with a high frequency. Hence, the action of the oscillating force is equivalent to the action of a point force dipole with intensity

$$M = J\epsilon = 4\pi^{5/2}\mathrm{d}\nu^{1/2}\epsilon^2 f^{3/2}. \tag{16}$$

This expression is used below for the quantative characterization of the source intensity in the laboratory experiments. Although formally its validity is restricted to cases $\epsilon \ll d$, it is assumed that (16) also applies to cases $\epsilon \approx d$ as occurs in the experiments described in the next sections.

The main overall characteristics of the quadrupoles, i.e. their maximum width D and their maximum length L, were measured throughout the course of the experiment from the dye pattern as shown schematically in figure 1. The experiments were conducted at moderate values of the Reynolds number (in the range 160–2200, see table 1). For $Re > 2500$ the motion in the vicinity of the rod was observed to become three-dimensional and the flow is then unstable: the primary frontal vortices are formed periodically (see also Tatsuno & Bearman 1990, figure 13). At $Re \lesssim 100$ the quadrupoles develop very slowly, and even the slightest background motion strongly disturbs the symmetric shape of the generated quadrupolar flow. For this reason attention was focused on the region of intermediate Re-values, for which reliable data could be obtained.

The array of quadrupolar vortices was created by a horizontally oscillating grid, consisting of vertical rods of diameter $d = 0.07$ cm placed equidistantly in a linear array of length $D_0 = 20$ cm. Three different grids of the same length were used, with rod spacings $d_0 = 0.5$, 1.0 and 2.0 cm, respectively. One of the grids was positioned vertically in the upper layer, with the polished ends of the rods just above the interface between the layers. As for the oscillating rod, the grid was fixed to a light, but rigid, horizontal frame that could oscillate horizontally in the direction normal to the grid plane with an adjustable frequency f and amplitude ϵ. The oscillation frequency was 9, 15 or 18 Hz, and the amplitude was varied in the range 0.09–0.19 cm. For all the experimental runs carried out, the values of the various parameters are listed in table 2. Again the resulting motion in the upper layer was visualized by adding the pH-indicator thymol blue to the fluid. Prior to each experiment, a few drops of basic fluid were introduced near the grid, thus locally providing a dramatic colour contrast.

Two types of oscillating-grid experiments were performed. In the first case the grid was placed in the centre of the container, so that the ends of the grid were relatively far (*c.* 8 cm distance) from the sidewalls of the container. This geometry was chosen to examine quantitatively the influence of the sidewalls on the mean large-scale motion

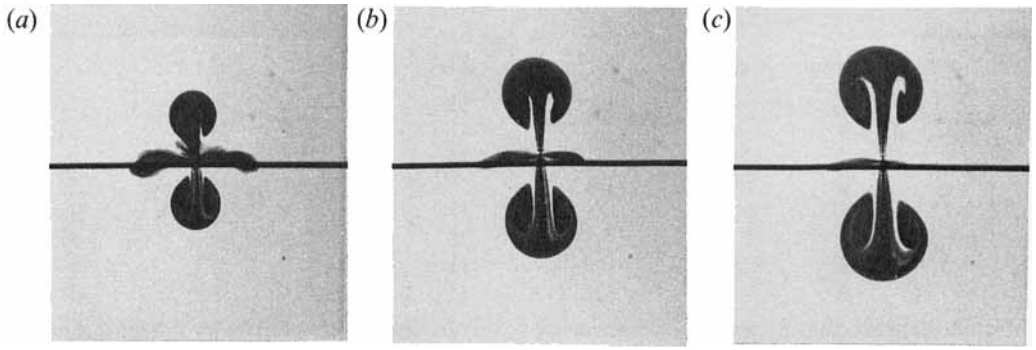

FIGURE 6. Sequence of planview photographs showing the formation and subsequent evolution of a symmetric vortex quadrupole induced by a rapidly oscillating cylinder. This cylinder is fixed to the supporting bar, which is visible on the photographs as the dark line. Experimental parameters: $f =$ 9 Hz, $\epsilon = 0.14$ cm. The photographs were taken at (*a*) $t = 4.4$ s, (*b*) 9.2 s, (*c*) 13.2 s after the forcing was started.

that develops. In the second case, two additional parallel walls were introduced into the container to form a long channel with width equal to the length of the grid (20 cm). In this case the grid completely spans the channel width and so any mean large-scale motion is practically absent. The quantitative data on the flow evolution and the propagation of the fronts of the turbulent region that arises were obtained only in this latter geometry.

4. Experimental results and interpretation

4.1. *Single quadrupoles*

The typical evolution of the flow induced by the oscillating cylinder can be observed in the sequence of plan-view black-and-white photographs presented in figure 6 (see also figure 5, plate 1). In the photographs the black line is the supporting rod to which the cylinder is fixed. The cylinder itself is not visible, because it points downwards into the fluid; it performs a horizontal oscillating motion in a direction perpendicular to the axis of the supporting rod. At the start of the experiment some dye was present near the cylinder (some traces can still be observed in the photographs); most of this dye is seen to get carried away in the two symmetric dipolar vortices that are formed after the oscillations start. The two dipolar vortices move away from the source of motion along aligned, straight trajectories; their size is observed to increase gradually, while their translation speed decreases. Once the dipolar vortices have moved sufficiently far away from the origin, the flow in the vicinity of the source can be considered as being steady. This can be observed on the streak photographs presented in figure 7: once the dipolar vortices (still visible in figures 7*a* and 7*b*) have left the source region, the flow takes on a steady appearance (see figures 7*c* and 7*d*), consisting of two outflow regions in the form of narrow jets in the oscillation direction and two wide inflow regions. In the flow field near the source the azimuthal velocity component (referring to a polar coordinate system with the origin coinciding with the source position) is negligibly small, and the tracer particles move along nearly straight radial lines, both in the inflow and in the outflow regions. The ultimate steady quadrupolar flow was studied analytically by Voropayev (1994) and in the present paper attention is mainly focused on the

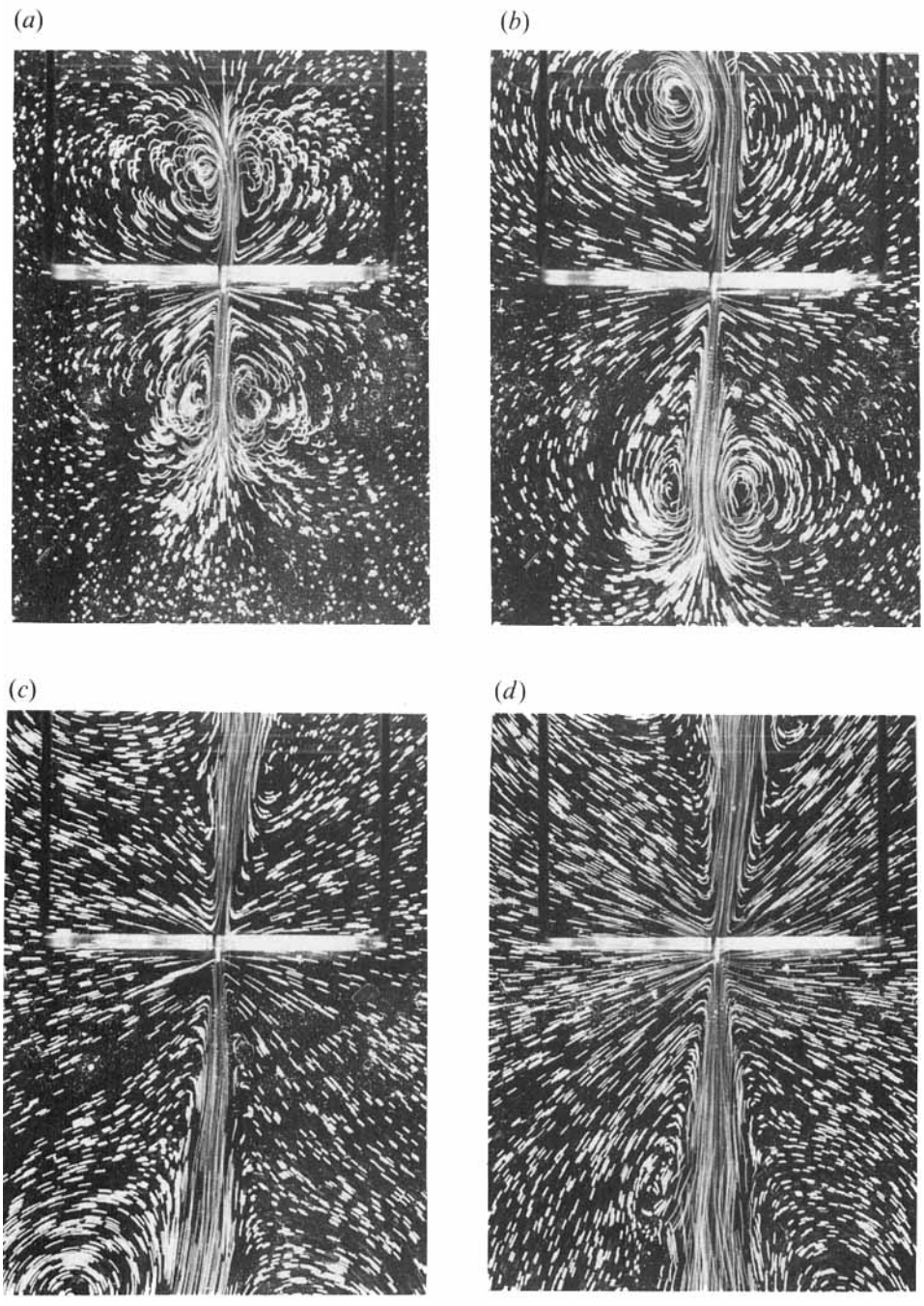

FIGURE 7. Streak photographs showing the evolution of the quadrupolar vortex induced by an oscillating cylinder. The rectangular construction visible in the pictures is the supporting frame to which the cylinder is attached. Experimental parameters: $f = 9$ Hz, $\epsilon = 0.14$ cm. The photographs were taken at (*a*) $t = 4$ s, (*b*) 10 s, (*c*) 15 s, (*d*) 30 s, and the exposure time was 2 s.

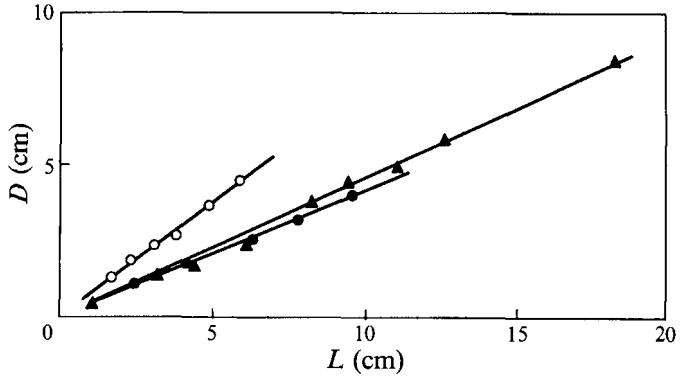

FIGURE 8. Graphical presentation of measured values of the width D of the quadrupolar vortex for different distances L from the origin for experiments 8 (○), 23 (▲) and 15 (●). Experimental parameter values are listed in table 1.

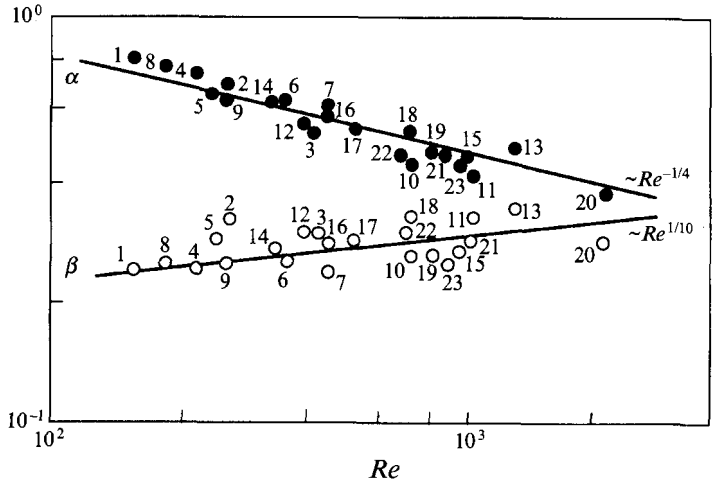

FIGURE 9. Measured values of α in (5) and β in (8) for different values of the Reynolds number Re. The numbers in the graph refer to the experiments listed in table 1. The solid lines represent the relationships (17) and (18).

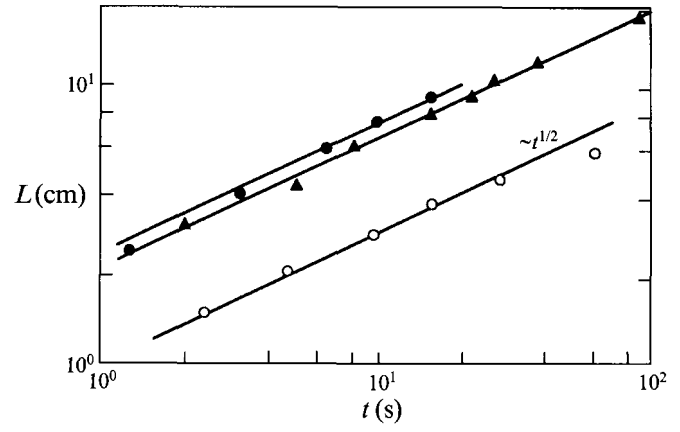

FIGURE 10. Measured values of the length L for different times t for experiments 8 (○), 23 (▲) and 15 (●). Experimental parameter values are given in table 1.

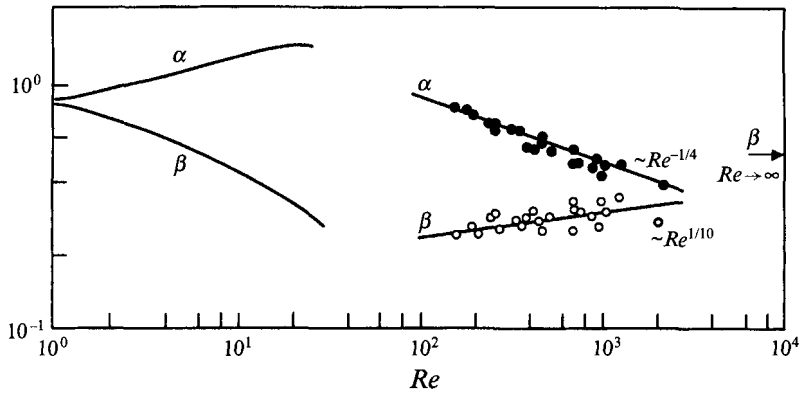

FIGURE 11. The behaviour of α and β in a wide range of Re-values. The solid lines represent the theoretical estimates (12) and (14) for small Re-values, and the approximations (17) and (18) of the experimental data (dots) for large Re-values. The transition region at moderate Re-values remains unstudied.

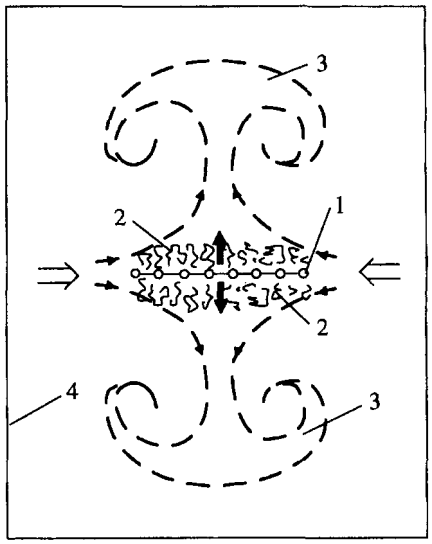

FIGURE 12. Schematic drawing of the flow generated by an oscillating grid with the tank sidewalls far from the edges of the grid. The numbers indicate: 1, the grid; 2, the region of small-scale vortical motions near the grid; 3, the induced large-scale quadrupolar flow, which is governed by the total intensity $M_0 = MD_0/d_0$ of the grid forcing; 4, the container. The open arrows indicate the inflow of ambient fluid near the ends of the grid.

intermediate-asymptotic stage (see figure 6), which appears too complicated to study analytically.

Two main characteristics of the flow were measured in the experiments: the maximum width D and the distance L from the origin to the front of the dye structure (see figure 1). Typical experimental data for D and L obtained during three different experiments are shown graphically in figure 8. All measurements were made at $L/l \lesssim 0.6$, where $2l$ is the length of the container, and the source is placed at the middle of the tank. In order to estimate the influence of the tank walls on the measurements results one can use (1). For $r \gtrsim L$ the velocity at the point $(r, \frac{1}{2}\pi)$ can be written as $u + u_0$, where u and u_0 are the velocities induced by the source and its mirror image,

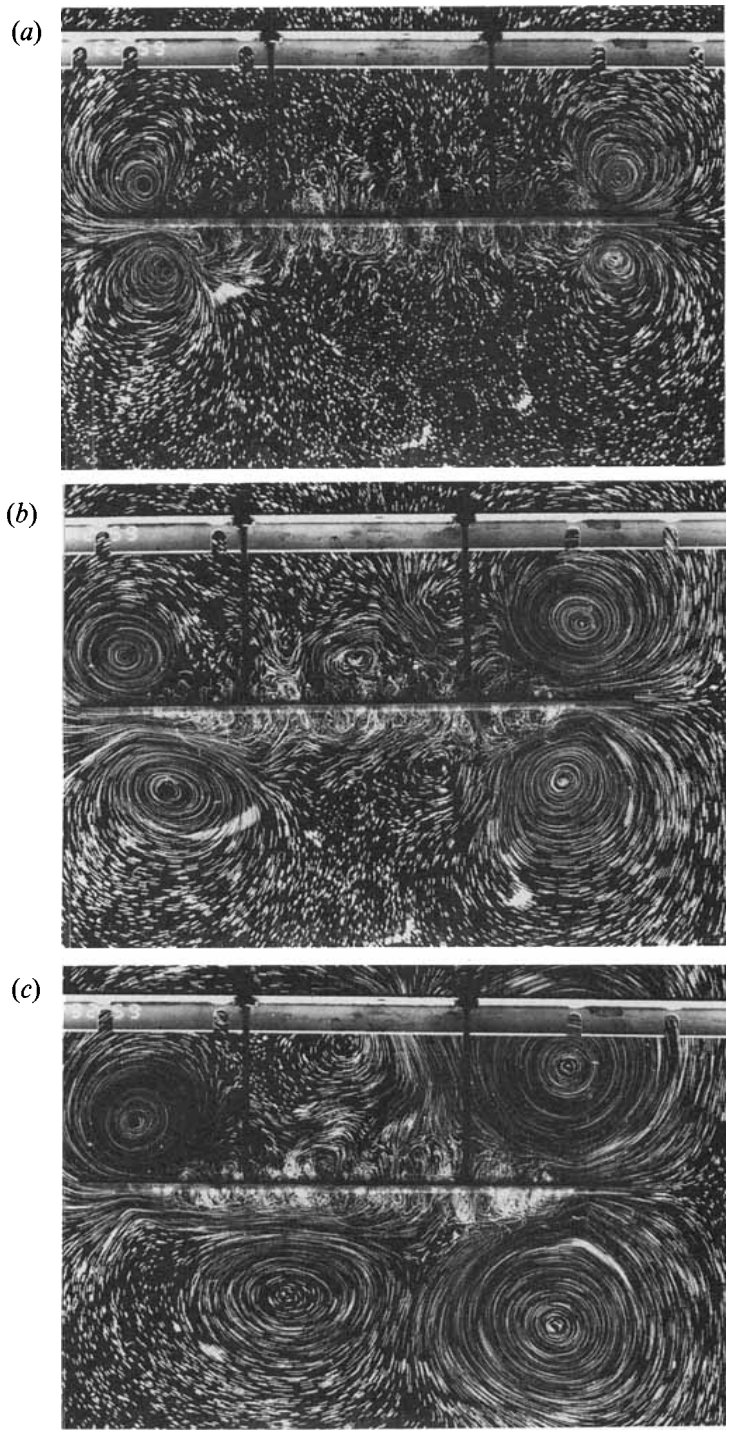

FIGURE 13. Sequence of streak photographs of the flow generated by the oscillating grid with the tank walls far from the grid ends ($h/D_0 \approx 1.8$, with h the width of the container and D_0 the length of the grid). Experimental parameters: $d_0 = 1$ cm, $\epsilon = 0.13$ cm, $f = 18$ Hz, exposure time 2 s. The rectangular construction visible in the upper part of the pictures is the supporting frame to which the grid is attached.

respectively. Using (1*a*) one obtains the upper estimate: $u_0/u = r^3/(2l-r)^3$. For $r/l \lesssim 0.6$ this gives $u_0 \lesssim 0.06u$.

To demonstrate that the size of the working container does not influence the experimental results, two sets of experimental data, 15 and 23, obtained in smaller and larger containers at approximately the same *Re*-values are presented together in figure 8. It is found that the experimental data are in good agreement with the linear relationship (5); the mean values of the proportionality coefficient α in (5) have been determined for the 23 experiments listed in table 1, and the results are plotted in figure 9 as a function of the Reynolds number *Re*. The straight line in this graph represents the approximation to the data by a conjectured power relationship of the form

$$\alpha = c_1 Re^{-1/4}, \tag{17}$$

where the proportionality constant is $c_1 = 2.5 \pm 0.3$.

In order to verify the relation (8) the dependence of L on time t was measured in all experiments listed in table 1. Some typical results of the measurements obtained in the same experiments as those of figure 8 are presented in figure 10, and a good agreement with a power law $L \sim t^{1/2}$ (denoted by the straight lines) can be observed. The proportionality coefficients in this relationship were estimated from these data, and this yielded values of the function $\beta(Re)$ in (8) for all 23 experiments. The results are presented graphically in figure 9, together with those of α, as a function of the Reynolds number *Re*. The straight line through the β-data in figure 9 represents the approximation of the data by a conjectured power relationship of the form

$$\beta = c_2 Re^{1/10}, \tag{18}$$

where the proportionality constant is $c_2 = 0.14 \pm 0.02$.

The corresponding functions $\alpha(Re)$ and $\beta(Re)$ were also determined experimentally for single vortex dipoles by Voropayev *et al.* (1991, figure 11). It is not possible to compare the data for the functions $\alpha(Re)$ and $\beta(Re)$ directly, because the forcing and the definition of β is different for the dipole and the quadrupole flow. (In the case of the quadrupole the linear solution (1) was used to estimate the velocity scale (4), in contrast to the case of the dipole where the nonlinear solution obtained for the steady jet in the boundary-layer approximation was used.) Nevertheless, the functions α and β for these two types of flow are qualitatively similar in that in both cases the functions $\alpha(Re)$ show a rapid decrease with *Re* and the functions $\beta(Re)$ show a slight increase with *Re* at large *Re*-values.

Thus, the planar quadrupolar flow develops in a self-similar manner not only at small, but also at large *Re*-values. The only governing parameter in this flow is the non-dimensional intensity (*Re*) of the force dipole, which determines the main characteristics of the flow. Some of these characteristics can be estimated using only two non-dimensional functions $\alpha(Re)$ and $\beta(Re)$, which have been determined theoretically (for small *Re*-values) and experimentally (for large *Re*-values), the results being summarized graphically in figure 11. The transition region at moderate *Re*-values (10–100) remains unstudied. Below, the results obtained for single quadrupoles are used to explain the experimental data for the evolution of the array of quadrupoles.

4.2. *Array of quadrupoles*

4.2.1. *Large-scale motion*

Consider first the flow induced by the grid when its ends are far from the sidewalls of the container (see figure 12). After the grid oscillation is started, each individual oscillating rod acts on the fluid as a localized force dipole with intensity M per unit

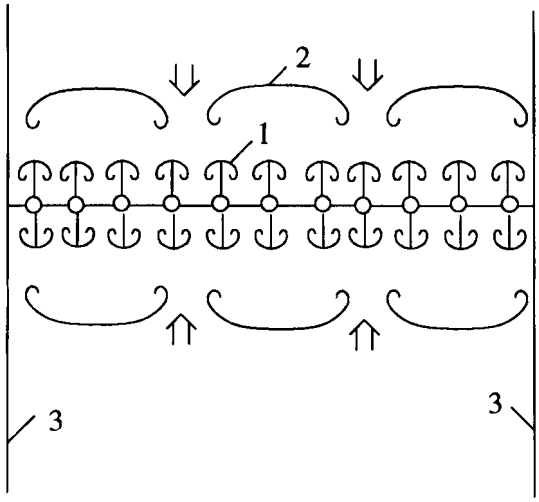

FIGURE 14. Schematic drawing of the flow generated by an oscillating grid stretched across the width of the channel. The numbers indicate: 1, primary quadrupoles; 2, the region where the primary quadrupoles intensively interact, forming larger secondary vortex structures; 3, channel walls. The open arrows indicate the entrainment of ambient fluid.

immersed rod length, given by (16). Thus, the action of the oscillating grid can be considered as a distributed force dipole of total intensity $M_0 = MD_0/d_0$ (with D_0 the grid length and d_0 the spacing between the rods), and at large distances the flow must be similar to that produced by a single force dipole with intensity M_0. In accordance with (1) the far-field flow has a quadrupolar character with the stream function given by

$$\psi_0 \approx \lim_{\xi \to \infty} \psi = -\frac{M_0 t}{2\pi r^2} \sin 2\theta.$$

In an incompressible fluid this large-scale motion is induced instantaneously by the action of pressure forces. This motion is very intensive (in the experiments D_0/d_0 ranged from 10 to 40, hence $M_0 \gg M$). As a result, the vorticity produced by each rod is swept by the large-scale motion (figure 12), leading to the rapid formation of four large vortices (figure 13*a*). With time the flow in the confined geometry becomes quasi-steady: irregular small-scale motions are localized in a small region near the grid, while four large vortices exist at some distance away. Although these large cells show some weak drift about a mean position, the four-cell pattern is quite stable (see figure 13*b*, *c*). Qualitatively such a flow is very similar to the quasi-steady streaming induced by an oscillating cylinder in a small tank (see Schlichting 1955 and Van Dyke 1982, figure 31).

Thus, the oscillating grid in the considered geometry induces an intense large-scale quadrupolar circulating motion.

4.2.2. *Formation and evolution of turbulent region*

To eliminate the large-scale motion, the grid was placed in the middle of a channel such that it spans the whole width of the channel (see figure 14). In this geometry the grid does not produce any significant large-scale motion and after the grid oscillation is started, the action of the grid can be characterized as a linear arrangement of force dipoles. This forcing gives rise to a linear array of vortex quadrupoles, as can be clearly seen in figure 15(*a*). In the initial stage of the experiment (1–2 s), when the typical width

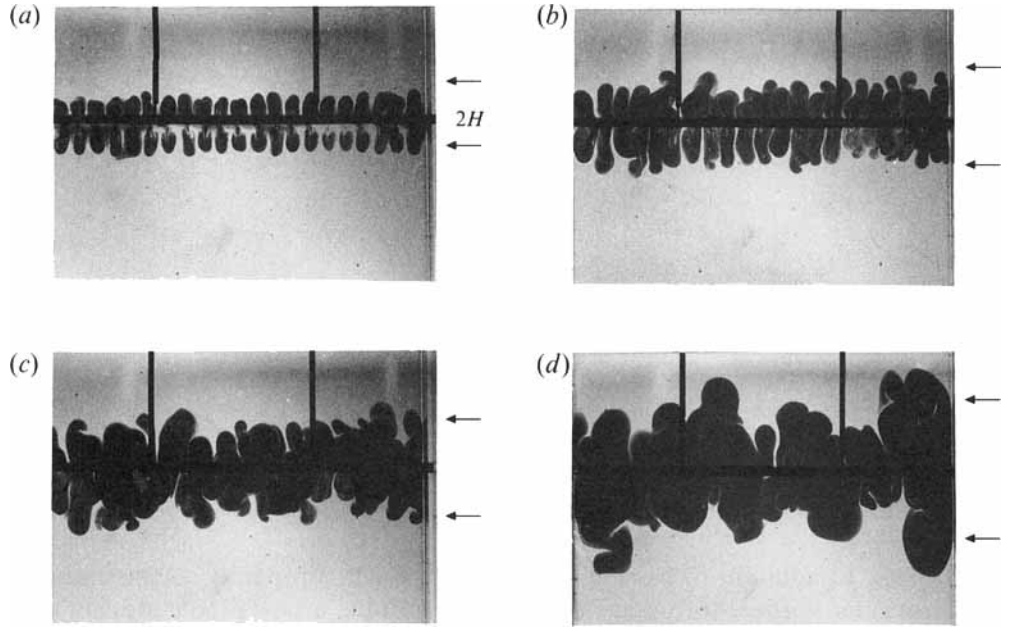

FIGURE 15. Sequence of photographs showing the evolution of the flow generated by a horizontally oscillating linear grid of vertical rods in a rectangular channel when the grid spans the whole width of the channel. The forcing was started at $t = 0$, and the photographs were taken at (*a*) $t = 1.3$ s, (*b*) 3.2 s, (*c*) 5.5 s, (*d*) 19 s. Experimental parameters: $d_0 = 1$ cm, $d = 0.07$ cm, $\epsilon = 0.13$ cm, $f = 18$ Hz, $Re = 530$. Just before the start of the experiment the fluid in the vicinity of the grid was dyed. The arrows indicate the mean positions of the vortical fronts.

D of the vortex structures is still less than the rod spacing d_0, the primary quadrupoles develop independently (see figure 15*a*). As time progresses, the quadrupole size D gradually increases, and when D becomes comparable with the spacing distance d_0 the quadrupoles start to interact (see figure 15*b*). At this stage the explicit order is lost and the flow is irregular or turbulent (figure 15*c*, *d*); the short initial stage is over and the prolonged (many tens of seconds) intermediate stage beings. At this stage the irregular two-dimensional motions are confined to a limited region with well-defined sharp boundaries. The width H of this region, indicated by the arrows in figure 15, increases with time, its boundaries propagating in opposite directions away from the grid into the irrotational ambient fluid. The limited size of the turbulent region, i.e. its well-defined width H, provides an easily measurable characteristic of this two-dimensional turbulent flow.

The visual observations revealed a rather complex picture of motions in the turbulent region. The primary vortices generated on either side of the grid visually do not interact directly with their counterparts on the other side of the grid (note, however, that the flows on the opposite sides of the grid influence one another by pressure forces, as in the case of a single quadrupole). Observations revealed that these primary vortices mostly interact directly with the vortices generated on the same side of the grid by the nearest rods. Two neighbouring primary dipoles usually merge, thus forming a larger secondary dipolar structure that detaches from the source of motion and moves away from the grid. At the same time a new primary structure begins to grow in the vicinity of the rod and this process is repeated. The size of the secondary structures gradually increases owing to the entrainment of ambient fluid and

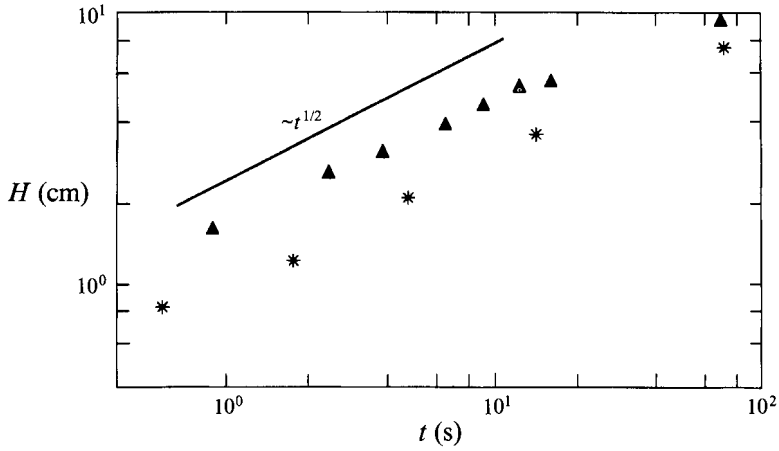

FIGURE 16. Measured values of the width H of the turbulent region as a function of time t for experiments 3 (*) and 8 (▲). Experimental parameter values are listed in table 2.

interactions. In addition to pairing, two dipoles, moving in parallel, sometimes split and their inner vortices (of opposite sign) join, forming a new dipole moving in the opposite direction (i.e. 'backwards').

Tripolar, quadrupolar and more complex structures are sometimes visible in the turbulent region, but the most frequently occurring structure is the dipolar vortex. The interaction/pairing process is repeated continuously, leading to the formation of even larger tertiary structures and causing the vorticity front to propagate into the irrotational surrounding fluid. Ambient fluid is entrained periodically into the turbulent region between large leading structures (see figure 15). It spreads in this region in the form of narrow long filaments and gradually gets entrained into the vortex structures, as can be seen from the spiral-shaped dye distributions. The vorticity diffusion across these spirals is very effective and soon the entrained fluid becomes vortical.

The dynamics of the turbulent region can be characterized by its global behaviour, e.g. by the width $H(t)$ of the turbulent region. Experimentally, this width is determined by measuring the mean position of the front of the dyed region relative to the grid. To derive an estimate of $H(t)$, let us assume that the width H of the turbulent region does not depend on the intensity M of the forcing due to single rods, but rather depends on the *mean force intensity* $m = M/d_0$ per unit grid length. It is then possible to write H as a function of three external parameters:

$$H = f(m, \nu, t). \tag{19}$$

The dimensions of the quantity m are L^3T^{-2}. By applying a dimensional analysis, (19) can be written as

$$H = m^{1/3} t^{2/3} \Phi(\eta) \quad \text{with} \quad \eta = mt^{1/2}/\nu^{3/2}, \tag{20}$$

where Φ is a non-dimensional function of the non-dimensional variable η. The typical evolution of $H(t)$, as measured in two different experiments, is shown in figure 16. In the first approximation, the data suggest that $H \sim t^{\gamma}$, with $\gamma \approx \frac{1}{2}$. To satisfy this experimental result, the function $\Phi(\eta)$ in (20) should behave as $\Phi(\eta) \sim \eta^{\lambda}$, with $\lambda = 2\gamma - \frac{4}{3}$. This would imply that

$$H = \text{const.}\, m^{2\gamma-1} \nu^{2-3\gamma} t^{\gamma},$$

which is clearly incorrect. For example, for $\gamma = \frac{1}{2}$ this gives $H \sim (\nu t)^{1/2}$, which is obviously independent of the main governing parameter m; this result also disagrees with the observations shown in figure 16. The choice $\gamma < \frac{1}{2}$, as suggested by some of the data sets, would lead to $H \sim m^{-\delta}$, with $\delta = 1-2\gamma > 0$, which is even more erroneous.

In order to obtain a realistic estimate of H, we should return to the full set of governing parameters. In general, the width H can be written as a function of five parameters:

$$H = f(M, D_0, d_0, \nu, t). \tag{21}$$

Since two of these parameters have independent dimensions, according to Buckingham's theorem the number of parameters in (21) can be reduced from five to three. This is, however, still a large number, and the chances of predicting the proper dependence are very small. Therefore it is useful, whenever possible, to take into account some physical arguments. For this purpose consider the initial stage of the flow evolution, when the primary vortex structures develop independently, without any direct mutual interaction. The typical length L and width D of the individual vortex quadrupoles increase with time according to (5) and (8), with α and β given by (17) and (18). By using these lengthscales, the dependence (21) can be written in non-dimensional form as

$$H/L = \phi(Re, D_0/D, d_0/D). \tag{22}$$

Note that both L and D are introduced in (22) for convenience: because L and D are related through the known function $\alpha(Re)$, formally only one lengthscale is used in (22). Since in the experiments $Re \gg 1$ and $D_0/D \gg 1$, it is assumed that the function ϕ possesses complete similarity with respect to the arguments Re and D_0/D, i.e.

$$\phi(Re \gg 1, D_0/D \gg 1, d_0/D) = \phi_0(d_0/D).$$

Hence, the estimate for H is

$$H = L\phi_0(d_0/D). \tag{23}$$

To determine the non-dimensional function $\phi_0(d_0/D)$ experimentally, in all experiments the argument d_0/D as well as the lengthscale L have to be normalized at the transitional point, $d_0/D = 1$, between the initial and intermediate-asymptotic stages. From the condition $d_0/D = 1$, with the help of (5), (8), (17) and (18) one obtains an estimate for the transition time:

$$t_* = \frac{d_0^2}{2c_1^2 c_2 Re^{3/5}\nu}. \tag{24}$$

By introduction of a non-dimensional time $\tau = t/t_*$, one can cast (23) in a normalized form, as

$$H_0 = \frac{c_1 H}{Re^{1/4} d_0} = \tau^{1/2}\phi_0(d_0/D), \tag{25}$$

where $\tau = 1$ at $d_0/D = 1$ and $c_1 = 2.5$, $c_2 = 0.14$ in accordance with (17) and (18).

At $\tau \lesssim 1$ (i.e. $t \lesssim t_*$) the primary vortices do not interact significantly but they develop independently. Hence, one may expect that during the initial stage the width H of the vortical region is equal to the length L of the single structures: $H = L$, which yields $\phi_0 = 1$ for $\tau \lesssim 1$. The experimental data obtained at small times ($t \lesssim t_*$) are plotted according to the non-dimensional form (25) in figure 17, with the solid line representing the estimate (25) with $\phi_0 = 1$. The best fit through the experimental data gives

$$\phi_0 = c_0 = 0.95 \pm 0.1 \quad \text{for} \quad \tau \leqslant 1, \tag{26}$$

which is in good agreement with the estimate $\phi_0 = 1$.

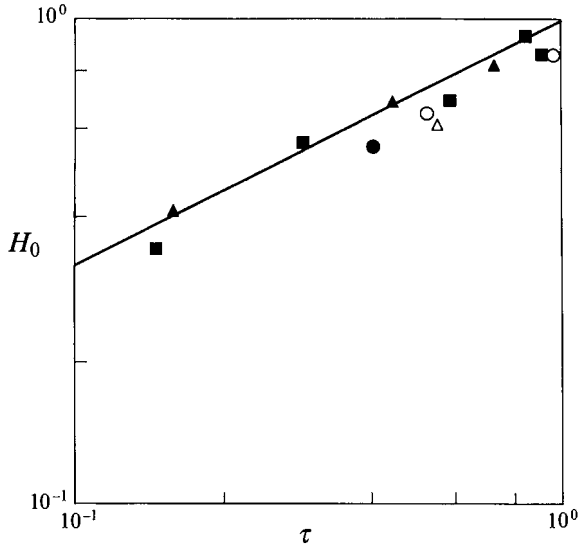

FIGURE 17. Experimental data representing the normalized non-dimensional width H_0 of the vortical region as a function of the normalized time τ for the initial stage ($\tau \leqslant 1$). The solid line represents the dependence (25) with the estimated value $\phi_0 = 1$. Experimental parameters are listed in table 2.

At $\tau = 1$ the initial stage is over, the primary vortices start to interact and the intermediate stage begins. At this stage the interactions play an essential role, the motion is now turbulent and ϕ_0 in (25) may differ from (26). To compare the experimental data obtained at this stage ($\tau > 1$) with (25), a small correction $(t+\Delta t)$ was introduced into the time origin. This was done because the origin of time in the experiment does not coincide with the time origin of the intermediate stage at $H \to 0$. The measurements yield values of Δt in the range 0–1 s, see table 2. These small corrections were introduced into all the data, obtained in eight experiments for $\tau > 1$, and the data were replotted according to the non-dimensional form (25). The result is presented in figure 18. Note that some of the scatter of the data points observed in a specific experiment, marked by one specific symbol, is due to the data being obtained in different tests under the same conditions. The solid line in this graph represents the estimate (25) with $\phi_0 =$ constant. The best fit through the 65 experimental points gives

$$\phi_0 = c = 0.6 \pm 0.1 \quad \text{for} \quad \tau > 1. \tag{27}$$

Summarizing, in a first approximation the function $\phi_0(d_0/D)$ in (25) can be represented by a step-like function given by (26) and (27) for $\tau \leqslant 1$ and $\tau > 1$, respectively.

It is hardly possible to estimate quantitatively the observed decrease in the value of ϕ_0 at the intermediate stage, and only a simple qualitative interpretation can be given. In two dimensions there is no stretching of vortex lines and the typical size of the leading structures at the front of the vortical region may only increase with the distance from the origin. The mean propagation velocity $\mathrm{d}H/\mathrm{d}t$ of the front (entrainment velocity) is determined by the rate of entrainment of irrotational ambient fluid into the turbulent region. As was pointed out above, this occurs mainly between large leading structures. When these structures are tightly packed, the rate of entrainment reduces, compared to the case of single structures, and the propagation velocity of the front diminishes. The fact that ϕ_0 at this stage is approximately constant means that the structure of the front is similar at different moments of time (self-similarity).

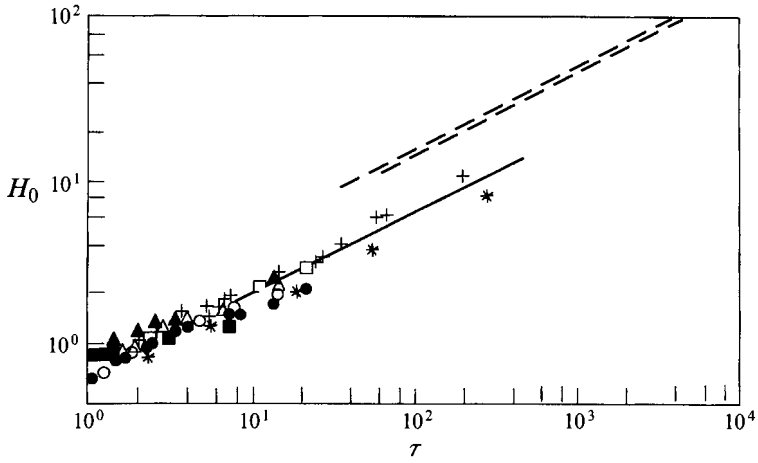

FIGURE 18. Experimental data representing the non-dimensional width H_0 of the two-dimensional turbulent region as a function of the normalized time τ for the intermediate stage ($\tau > 1$) for the eight experiments listed in table 2. The solid line represents the estimate (25) with $\phi_0 = 0.6$. The dashed lines represent the data obtained by Dickinson & Long (1978) in experiments with a plane oscillating grid, for three-dimensional geometry.

5. Concluding remarks and discussion

In summary it is concluded that a small cylinder, oscillating in the direction normal to its axis, acts on the fluid as a localized force dipole. It is shown that in a viscous fluid the action of the force dipole gives rise to the formation of a planar quadrupolar vortex flow of zero total momentum. The main governing parameter for this flow is the source intensity M (with dimensions L^4T^{-2}) determined by (16). This permits one to define the non-dimensional forcing as $Re = M/4\pi\nu^2$, where Re is the Reynolds number of the flow. The flow has no external lengthscale and develops in a self-similar manner: the length and the propagation velocity of the quadrupolar structure (marked by dye) change with time as $L \sim t^{1/2}$, $\bar{U} \sim t^{-1/2}$ and they are characterized by the non-dimensional functions $\alpha(Re)$ and $\beta(Re)$, respectively. These functions were determined analytically for small Re-values and experimentally for large Re-values.

The present study also demonstrates that quadrupoles are the basic primary flow elements induced by an oscillating grid in a two-dimensional geometry. After the oscillation is started, an array of quadrupoles, distributed regularly along the grid, arises. Initially, at $t \lesssim t_*$, where t_* is the transition time, the interactions are weak and these primary structures develop independently. Later, at $t > t_*$, the interactions play an essential role in the flow dynamics and the motion becomes turbulent over the whole width of the vortical region. During both stages the width H of the vortical flow region increases with time as $H \sim t^{1/2}$. It is shown that the main governing parameter here is the non-dimensional forcing, Re, as in the case of single quadrupoles, and the additional external lengthscale (the rod spacing d_0) does not enter directly into the dependence $H(t)$, but is introduced indirectly via the transition time t_*.

The physical arguments and the scaling analysis used to explain the propagation dynamics of a two-dimensional turbulent region are general enough to be applied to the three-dimensional geometry as well. To demonstrate this, consider the results of measurements reported by Dickinson & Long (1978). In their experiments a plane horizontal grid fabricated from a fine woven copper screen ($d_0 = 0.155$ cm, $d =$ 0.033 cm) was used to generate three-dimensional turbulence. This grid was oscillated

vertically in a deep tank with homogeneous fluid and it produced a horizontal turbulent layer of increasing depth $H(t)$. The amplitude of the oscillations was fixed, $\epsilon = 0.475$ cm, and in different experiments the oscillation frequency was varied in the range $f = 6.3$–12.0 Hz. The transition time t_*, given by (24), for these parameters is very short ($t_* \simeq 0.02$ s) and only the intermediate stage was studied. The measurements obtained in these experiments are presented in the non-dimensional form (25) in figure 18 and are shown by the two dashed lines between which points obtained in other experiments with different frequencies are situated. It is clear that the experimental data obtained in the different experiments practically lie on a single line, in agreement with (25). This gives for ϕ_0 in (25)

$$\phi_0 = c_3 = 1.3 \pm 0.05 \quad \text{for} \quad \tau > 1 \tag{28}$$

in the case of three-dimensional geometry. The difference in the values of ϕ_0 for two- and three-dimensional geometry is not surprising. In the latter case the motion can be considered as planar only in the close vicinity of the grid (at least, in the boundary layer near the rods) where no-slip conditions and viscous effects determine the amplitude of forcing, as given by (16). At greater distances the motion is essentially three-dimensional, an additional degree of freedom appears and ϕ_0 changes from the two-dimensional case.

To explain Dickinson & Long's (1978) data, Long (1978) introduced a quantity called the 'action' of the grid and proposed in his qualitative theory that the flow near the planar oscillating grid be modelled by a system of doublets of opposite sign placed regularly in infinitesimal holes in a rigid plane. Long's theory does not allow us to determine the dependence of the action K on external parameters: it only predicts that $K \sim f$. The values of K must be determined from the experimental dependencies

$$H = (Kt)^{1/2}.$$

Now, with the help of (8), (23) and (28), we can calculate Long's action as

$$K = 2c_3^2 \beta \nu \, Re \tag{29}$$

and compare the calculated values with those (K_{exp}) obtained experimentally by Dickinson & Long (1978). This comparison is shown in figure 19. Thus, Long's action acquires a clear physical sense: at the limit $Re \to \infty$ ($\beta \to$ const, see figure 11) the action is equal, in fact, to the forcing amplitude $K \sim M/\nu$. This gives $K \sim f^{3/2}$, in agreement with Dickinson & Long's experimental data.

Finally, note that despite the good agreement shown in figure 19, one important question remains: is ϕ_0 for $\tau > 1$ for the three-dimensional case a universal constant that does not depend on f, d and ϵ, as in the two-dimensional case? But this is a separate problem which is beyond the scope of the present study; some results will be published by Long (1994) and Voropayev & Fernando (1994).

Concluding, we must stress that the results obtained in the present paper for grid turbulence are valid only for fine grids, made from circular rods of small diameter and oscillating with high frequency and small amplitude. Only in this case can the forcing produced by the grid elements be considered as localized and only in this case is it possible to put different external parameters together and to calculate accurately the forcing amplitude. In most of the previous studies on three-dimensional grid turbulence, a grid made from solid bars of square cross-section (1×1 cm) was used. In this case it is hardly possible to obtain an analytically correct estimate for the forcing amplitude and different empirical dependencies without clear physical sense are used for these grids. That is why Dickinson & Long's (1978) data, the only data obtained with fine grid, were used to verify our predictions for three-dimensional geometry.

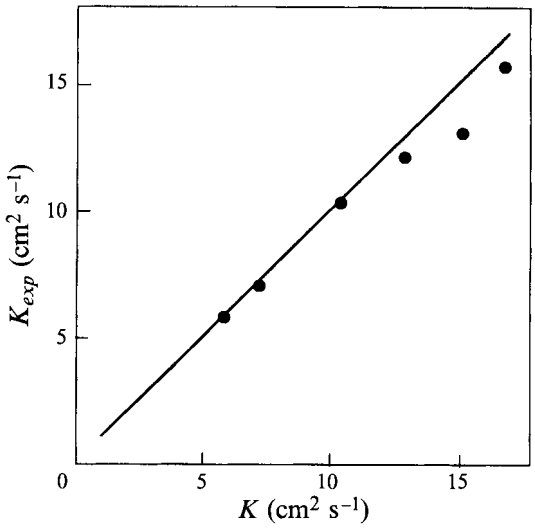

FIGURE 19. Comparison of the calculated grid action K according to (29) and the experimentally measured values K_{exp} of the grid action obtained by Dickinson & Long (1978) in experiments with $f = 6.3$, 7.2, 8.8, 10.0, 11.4 and 12.0 Hz. The solid line represents $K = K_{exp}$.

This research was carried out during a visit of two of the authors (S.I.V. and Y.D.A.) to the Fluid Dynamics Laboratory in Eindhoven, which was financially supported by the Dutch Organization for Scientific Research (NWO). The authors are indebted to Professor R. R. Long for very useful comments on this work and gratefully acknowledge the anonymous referees for their valuable comments on an earlier version of the paper. We thank Harm Jager and Cor Arends for their technical assistance. Thanks are also due to Prisca Koelman and Anita Peeters for the preparation of the typescript.

REFERENCES

AFANASYEV, YA. D. & VOROPAYEV, S. I. 1991 Plane vortex flow induced by a mass source (sink) in a rotating viscous fluid. *Fluid Dyn.* **4**, 618–621. (*Izv. Akad. Nauk SSSR, Mekh. Zhidk. Gaza*, translated from Russian.)

AFANASYEV, YA. D., VOROPAYEV, S. I. & FILIPPOV, I. A. 1988 Laboratory investigation of flat vortex structures in a stratified fluid. *Dokl. Akad. Nauk SSSR* **300**, 704–707.

BATCHELOR, G. K. 1967 *An Introduction to Fluid Dynamics*. Cambridge University Press.

CANTWELL, B. J. 1986 Viscous starting jets. *J. Fluid Mech.* **173**, 159–189.

DICKINSON, S. C. & LONG, R. R. 1978 Laboratory study of the growth of a turbulent layer of fluid. *Phys. Fluids* **21**, 1698–1701.

FERNANDO, H. J. S., HEIJST, G. J. F. VAN & FONSEKA, S. V. 1992 The evolution of an isolated turbulent region in a stratified fluid. *J. Fluid Mech.* (submitted).

FLÓR, J. B. & HEIJST, G. J. F. VAN 1994 Experimental study of dipolar vortex structures in a stratified fluid. *J. Fluid Mech.* **279**, 101–134.

HEIJST, G. J. F. VAN & FLÓR, J. B. 1989 Dipole formation and collisions in a stratified fluid. *Nature* **340**, 212–215.

LONG, R. R. 1978 Theory of turbulence in a homogeneous fluid induced by an oscillating grid. *Phys. Fluids* **21**, 1887–1888.

LONG, R. R. 1994 A theory of grid turbulence in a homogeneous fluid. *Phys. Fluids* (submitted).

SCHLICHTING, H. 1955 *Boundary Layer Theory*. McGraw-Hill.

SEDOV, L. I. 1959 *Similarity and Dimensional Methods in Mechanics*. Academic Press.

STERN, M. E. & VOROPAYEV, S. I. 1984 Formation of vorticity fronts in shear flow. *Phys. Fluids* **27**, 848–855.

TATSUNO, M. C. & BEARMAN, P. W. 1990 A visual study of the flow around an oscillating circular cylinder at low Keulegan–Carpenter numbers and low Stokes numbers. *J. Fluid Mech.* **211**, 157–182.

VAN DYKE, M. 1982 *An Album of Fluid Motion.* Parabolic Press.

VOROPAYEV, S. I. 1994 Steady two-dimensional quadrupolar flow: an exact solution of the Navier–Stokes equations and experiment. *J. Fluid Mech.* (submitted).

VOROPAYEV, S. I. & AFANASYEV, YA. D. 1992 Two-dimensional vortex-dipole interactions in a stratified fluid. *J. Fluid Mech.* **236**, 665–689.

VOROPAYEV, S. I., AFANASYEV, YA. D. & FILIPPOV, I. A. 1991 Horizontal jets and vortex dipoles in a stratified fluid. *J. Fluid Mech.* **227**, 543–566.

VOROPAYEV, S. I. & FERNANDO, H. J. S. 1994 Experiments on propagation of grid turbulence in a homogeneous fluid. *Phys. Fluids* (submitted).

VOROPAYEV, S. I. & FILIPPOV, I. A. 1985 Development of a horizontal jet in homogeneous and stratified fluids: Laboratory experiments. *Izv. Akad. Nauk SSSR, Fiz. Atmos. Okeana* **21**, 964–972.